New insight into crystal chemistry of topaz: A multi-methodological study

G. Diego Gatta,[1,*] F. Nestola,[2,3] G.D. Bromiley,[4] and A. Loose[5]

[1]Dipartimento di Scienze della Terra, Università degli Studi di Milano, Via Botticelli 23, I-20133 Milano, Italy
[2]Dipartimento di Mineralogia e Petrologia, Università degli Studi di Padova, Corso Garibaldi 37, I-35137 Padova, Italy
[3]Bayerisches Geoinstitut, Universität Bayreuth, Universitätsstrasse 30, D-95447 Bayreuth, Germany
[4]Department of Earth Sciences, Cambridge University, Downing Street, Cambridge CB2 3EQ, U.K.
[5]Forschungszentrum Jülich, D-52425 Jülich, Germany

Abstract

The crystal chemistry of a natural topaz [with $OH/(OH + F) < 0.5$] was reinvestigated by means of laser ablation inductively coupled plasma mass spectroscopy, single-crystal X-ray diffraction (at 298 K) and neutron diffraction (at 298 and 10 K), and polarized infrared spectroscopy to define unambiguously the real symmetry of topaz, the location of the proton and its thermal displacement parameters at room and low temperatures, the hydrogen-bonding and the vibration modes (stretching and bending) of the OH dipole. X-ray and neutron structural refinements allow us to infer that the crystal structure of natural topaz with $OH/(OH + F) < 0.5$ can be described with the *Pbnm* space group. Violating reflections, found in the previous investigations and in this study, are likely due to Renninger effect (double diffraction phenomenon). The nuclear density Fourier map shows that the proton is located at Wyckoff 8*d* position and the refined coordinates are: $x = 0.495(2)$, $y = 0.252(1)$, $z = 0.1629(7)$. The O-H bond lies on the (010)-plane and forms an angle of about 28.9° with the *c*-axis. Neutron structural refinements at 298 and 10 K show that the displacement ellipsoid of the proton is highly anisotropic. The H-bonding arrangement appears to be complex, with at least four potential H⋯O/F interactions (distances < 2.38 Å). The topological configuration of the O-H group described by the neutron structural refinements is confirmed by the infrared investigation: the OH stretching mode (at 3640 cm⁻¹) has no component of vibration parallel to the *b* axis (i.e., the O-H direction is perpendicular to [010]). The OH bending mode (at 1161 cm⁻¹) shows components along the three crystallographic axes, which appear to be more prominent along the *a* and *b*-axes. The possible distribution into the crystal structure of topaz of the minor/trace elements found (Na, Ca, Fe Cr, V, Ti, B), and the implied topological effects, is discussed.

Keywords: Topaz, crystal chemistry, plasma mass spectroscopy, X-ray and neutron diffraction, infrared spectroscopy

Introduction

Topaz [ideal formula $Al_2SiO_4(F,OH)_2$] is one of the most important F/OH-bearing silicates, and is found as accessory mineral in F-rich granitic rocks (or in detrital sediments near areas of acid intrusive rocks) associated with pneumatolithic/hydrothermal events and in ultrahigh-pressure rocks (Pichavant and Manning 1984; Taylor 1992; Taylor and Fallick 1997; Zhang et al. 2002; Alberico et al. 2003). Topaz is a stable phase above 12 GPa and 1100 °C and could play an important role in water sequestration in deeply buried continental crust (Holland et al. 1996; Domanik and Holloway 1996; Schmidt et al. 1998; Zhang et al. 2002). Due to its hardness (H8, Mohs' scale), topaz is used as heavy material for ornamental purposes, for the manufacture of abrasives, grindstones, sharpening stones, and scouring powders.

The crystal structure of natural topaz was independently solved by Alston and West (1928) and Pauling (1928) and reinvestigated by several authors (Ladell 1965; Ribbe and Gibbs 1971; Zemann et al. 1979; Parise et al. 1980; Alberico et al. 2003). Topaz is an ortho-silicate and its structure consists of chains of edge-sharing $Al(O,F,OH)_6$-octahedra connected by

isolated SiO_4-tetrahedra (Fig. 1). The proton lies in a cavity adjacent to the $Al(O,F,OH)_6$-octahedra (Fig. 1) and is associated with the F/O4 atom. The crystal chemistry and physical properties of topaz have been extensively investigated along the solid solution $Al_2SiO_4F_2$-$Al_2SiO_4(OH)_2$ by means of optical microscopy, IR spectroscopy and X-ray diffraction (Rinne 1926; Isetti and Penco 1967; Ribbe and Rosenberg 1971; Akizuki et al. 1979; Ribbe 1982 and references therein; Barton 1982; Barton et al. 1982; Belokoneva et al. 1993; Northrup et al. 1994; Wunder et al. 1993, 1999; Shinoda and Aikawa 1997; Bradbury and Williams 2003; Komatsu et al. 2003, 2005; Churakov and Wunder 2004; Gatta et al. 2006a). For natural topaz, with $OH/(OH + F) \leq 0.5$, the crystal structure was described in the *Pbnm* space group with one H-site (Fig. 1) (Alston and West 1928; Pauling 1928; Ladell 1965; Ribbe and Gibbs 1971; Zemann et al. 1979; Alberico et al. 2003). By contrast, Northrup et al. (1994) described the structure of the synthetic $Al_2SiO_4(OH)_2$ end-member [$OH/(OH + F) = 1.0$] in the *Pbn*2_1 space group, with two non equivalent and partially occupied (50%) H sites. The reduction of the symmetry (with a loss of the mirror plane) was adopted because of the close proton-proton distance (about 1.5 Å, Northrup et al. 1994). On the basis of a neutron powder diffraction data, Chen et al. (2005) refined
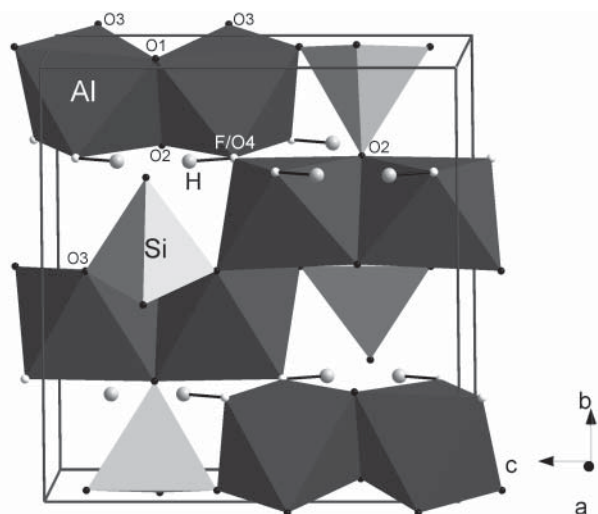
FIGURE 1. Clinographic view of the crystal structure of topaz. Atomic positions from Alberico et al. (2003).

the crystal structure of a fully deuterated topaz, $Al_2SiO_4(OD)_2$, in the *Pbnm* space group, reporting that the Rietveld refinement did not converge in *Pbn*2_1; two partially occupied deuterium sites (D1 and D2) have been found. However, even the crystal structure of natural topaz [OH/(OH + F) ≤ 0.5] has been the subject of debate concerning the topological configuration of the OH group and the real space group. On the basis of optical observations, and following the previous results of Rinne (1926), Akizuki et al. (1979) showed that natural topaz has pronounced sectoral textures. Sectors with general {*hkl*} growth planes have been found to be optically triclinic, whereas {0*kl*}, {*k*0*l*}, and {*hk*0} as optically monoclinic and {100}, {010}, and {001} as optically orthorhombic. The authors suggested that the lower symmetry is due to the non-random substitution of OH and F in the structure. However, they found no appreciable differences in F content from sector to sector. In addition, after heating at 950 °C for 4 h, the sample appeared to become homogeneously orthorhombic (i.e., heating caused F/OH-disordering). Parise et al. (1980) investigated the crystal structure of natural $Al_2SiO_4(F_{1.82}OH_{0.18})$ topaz by means of single-crystal neutron diffraction. Based on violation of the reflection conditions, the authors stated that the symmetry of topaz deviates from orthorhombic, suggesting *P*1 as a possible space group. The structural data were not reported, only the H-site coordinates (derived from the difference Fourier map) in the *Pbnm* and *P*1 space groups were given. Based on the observations of Azikuki et al. (1979), Parise heated the sample at 950 °C for 18 h, but the symmetry did not invert to orthorhombic (in Ribbe 1982). A single-crystal neutron diffraction study of a natural $Al_2SiO_4(F_{1.44}OH_{0.56})$ topaz was also performed by Zemann et al. (1979), who did not report any violation of the *Pbnm* space group. In addition, the H-coordinates reported by Zemann et al. (1979) differ for more than 3σ from those reported by Parise et al. (1980).

On the basis of the potentiality of the current neutron facilities (Gatta et al. 2006b) and improvements in other analytical techniques, the aim of this work is to reinvestigate the crystal structure and crystal chemistry of a natural (OH,F)-topaz, with

OH/(OH + F) < 0.5, by means of wavelength dispersive system electron microprobe analysis (WDS-EMPA), laser ablation inductively coupled plasma mass spectroscopy (LA-ICP-MS), single-crystal X-ray and neutron diffraction, and polarized infrared (IR) spectroscopy to define unambiguously the real symmetry of topaz, the location of the proton(s), and its/their thermal displacement parameters at room and low temperatures, the hydrogen-bonding and the vibration modes (stretching and bending) of the OH dipole.

EXPERIMENTAL METHODS

A natural, pale yellow and transparent, gem-quality, prismatic single crystal (~3.2 cm³) of pneumatolithic/hydrothermal topaz from Ouro Preto, Minas Gerais, Brasil, kindly provided by the Italian collector Stefano Putignano (Termoli, Italy), was used in this study. A preliminary check of the crystal in polarized light showed that it was free of defects. The crystal was then cut into several pieces, to perform the chemical analysis, the X-ray and neutron diffraction experiments, and the IR measurements.

One piece of the single crystal of the topaz sample (300 × 200 × 90 μm³) was used for the WDS-EMPA using a fully automated JEOL JXA 8200 microprobe at the Bayerisches Geoinstitut (BGI). Major and minor elements were determined at 15 kV accelerating voltage and 15 nA beam current, adopting a counting time of 20 seconds. To reduce loss of water and fluorine under electron bombardment, the crystal was mounted in epoxy resin and a defocused beam was used. The reference standards employed for the chemical analysis were: orthoclase (Si, TAP), spinel (Al, TAP), periclase (O, LDE1), and fluorite (F, LDE1). We measured the amount of oxygen to define the OH content. The final chemical formula (obtained by averaging 40 points analyses and on the basis of 2 apfu of Al) is $Al_{2.00}Si_{1.07}O_{4.26}F_{1.74}$, which can be rewritten as $Al_{2.00}Si_{1.07}O_{4.00}(OH_{0.26}F_{1.74})$.

Fine chemical analysis was performed on a second piece of the single crystal of topaz (400 × 300 × 110 μm³) by means of LA-ICP-MS at the Earth Science Department, University of Perugia, Italy, with a laser ablation system made by New Wave UP213 (Nd:YAG laser source) coupled with ICP-MS Thermo Electron X7. Calibration was performed using NIST SRM 612 as external calibrant in conjunction with internal standardization using ^{29}Si, previously measured in WDS-EMPA (Longerich et al. 1996). The data acquisition parameters (quadrupole settling time, dwell time, points per spectral peak) were optimized according to Longerich et al. (1996), and the protocol and data reduction algorithms suggested by Longerich et al. (1996) were adopted. The following masses (isotopes) have been analyzed: ^7Li, ^{11}B, ^{23}Na, ^{24}Mg, ^{39}K, ^{44}Ca, ^{45}Sc, ^{47}Ti, ^{51}V, ^{52}Cr, ^{56}Fe, ^{71}Ga and ^{133}Cs. The final chemical composition is reported in Table 1.

Doubly polished sections of the topaz sample were prepared for examination of the OH stretching and bending modes using FTIR spectroscopy at the Department of Earth Sciences, University of Cambridge, U.K. To this end, two small single crystals were previously oriented using a Huber four-circle X-ray diffractometer at the BGI, and then cut and polished in thin platelets with the polished surfaces parallel to (100) and (010) respectively. Sections were prepared using Crystalbond (TM), and polished to thicknesses of 15 and 17 μm. Prior to IR examination, sections were soaked for 24 hours in high-purity acetone. Polarized mid-infrared spectra were obtained using a Bruker IFS-66V spectrometer with a Globar MIR source, KBr beamsplitter, an MCT detector, and a wire-strip polarizer. 512 spectra were obtained for each measurement, using a resolution of 2 cm⁻¹. Samples were placed over a pin-hole aperture on a sample holder, orientation verified by optical microscopy, and the sample holder was then placed in the internal sample chamber of the spectrometer. The sample chamber was evacuated at high vacuum prior to obtaining spectra to prevent the appearance of anomalous absorption bands due to water vapor and CO_2. IR spectra were obtained from two sections using radiation polarized parallel to the *a*, *b*, and *c* crystallographic axes of the topaz sample. The high water content present in the topaz sample presented problems with detector saturation. To overcome these problems, the sections were polished down to the minimum thickness required to remove them from the glass slides without fracturing. However, even at thicknesses down to 15 μm, some of the OH bands in the MIR spectra were still saturated. Final spectra were, however, of sufficient quality to allow comparison with previous investigations, and it was still possible to determine the anisotropy of the main OH bands.

A single crystal of topaz (160 × 110 × 20 μm), optically free of twinning and other defects, was used for the X-ray diffraction experiment. Accurate lattice constants were first measured with a Huber four-circle diffractometer (non-mono-

TABLE 1. Chemical composition of the topaz sample

	wt%	Atoms pfu (on the basis of 2 apfu of Al)		wt ppm		wt ppm
Si	15.99(8)	1.07(1)	[7]Li	0.22(6)	[47]Ti	56(7)
Al	28.72(10)	2.00	[11]B	13(1)	[51]V	6.8(3)
F	17.66(12)	1.74(2)	[23]Na	240(15)	[52]Cr	67(4)
O	36.24(13)	4.26(2)	[24]Mg	2.1(4)	[56]Fe	24(2)
Tot.	98.61	$(Al_{2.00}Si_{1.07}O_{4.26}F_{1.74})$	[39]K	5.2(8)	[71]Ga	1.8(1)
			[44]Ca	634(61)	[133]Cs	0.10(4)
Final chemical formula:			[45]Sc	1.47(3)		
$Al_{2.00}Si_{1.07}O_{4.00}(OH_{0.26}F_{1.74})$						

Notes: Major elements were determined by WDS-EMPA and minor elements by LA-ICP-MS (Al_2O_3 wt% determined by WDS was used as internal standard for the LA-ICP-MS, see text). Standard deviations are in parentheses.

chromatized MoKα radiation) at the BGI using eight-position centering of 30 Bragg reflections (5° < 2θ < 40°), following the protocol reported by King and Finger (1979) and Angel et al. (2000). After the peak scanning and centering procedure, accurate unit-cell parameters were determined by vector-least-square refinement according to Ralph and Finger (1982) and Angel et al. (2000). The crystal was found to be metrically orthorhombic with $a = 4.6601(2)$, $b = 8.8260(2)$, and $c = 8.3778(2)$ Å. The unrestrained cell constants deviated from the constrained values less than 1.5 σ. On the basis of the correlation equation between wt% of F (w_F) vs. unit-cell constants (based on 29 data available in literature, according to Alberico et al. 2003), the value of the a-axis gives rise to a $w_F = 16.97(6)\%$, slightly lower than the value obtained from the WDS analysis [$w_F = 17.66(12)\%$, Table 1]. Diffraction data for the structural refinement were then collected at the BGI on an Xcalibur-Oxford Diffraction diffractometer (Kappa-geometry, graphite-monochromated MoKα radiation, point detector). Details concerning the data collection are summarized in Table 2. No restraints, in terms of the reflections conditions, were applied during the data collection. On 1455 collected reflections (maximum 2θ = 70.12°), 20 systematic absence violations of the *Pbnm* space group, belonging to the classes 00*l* (with *l* = 2*n* + 1), 0*kl* (with *k* = 2*n* + 1) and *h0l*, have been found. To define the nature of the violating reflections, we performed an azimuthal ψ-scan for each of them. All the violating reflections were very sharp (with a FWHM 20% smaller than the other reflections) and vanished after an azimuthal rotation of only 1.5–2.5°. Therefore, they might be ascribed to Renninger effect (double diffraction phenomenon). Integrated intensity data (corrected for Lorentz-polarization effects) were then obtained using WinIntegr3.4 program (Angel 2003a, 2003b) and the absorption correction was performed following the protocol of Burnham (1966) using the ABSORB5.2 computer program (Angel 2002). After correction, the discrepancy factor for the symmetry related reflections was $R_{int} = 0.0269$.

The last piece of the topaz single crystal (2 × 3 × 4 mm³) was used for the neutron diffraction experiments at 298 and 10 K with a Huber four-circle diffractometer (SV28/1) installed at the DIDO reactor—Forschungszentrum Juelich (FZJ), Germany. A He-cryostat designed at the FZJ was used for the low-*T* experiment. The incident radiation [obtained using a Cu(200) single-crystal monochromator] with a constant wavelength of 0.87238(1) Å was used for the room- and low-*T* experiments. The neutron flux density was about 2.5·10⁶ n·s⁻¹·cm⁻² and the tangential beam tube gave rise to a very small background count rate (~5 s⁻¹). A total of 4446 reflections (of which 988 unique) were recorded at 298 K (maximum 2θ = 99.93°) and 4049 reflections (of which 632 unique) at 10 K (maximum 2θ = 82.26°). For both data collections, two standard reflections were measured with a frequency of 450 min throughout the experiment and the intensity variation was within their σ(*I*). Further details concerning the data collections are reported in Table 2. The systematic extinction rules in general agreed with the space group *Pbnm*. However, we observed 6 and 14 violating reflections for the data collections at 298 and 10 K respectively, belonging to the same classes of violating reflections observed in the X-ray diffraction experiment. Intensity of the diffraction data was corrected for Lorentz effect and no absorption correction was applied because of the composition and the dimensions of the sample. The discrepancy factors for the symmetry related reflections were $R_{int} = 0.0229$ and 0.0251 at 298 and 10 K, respectively (Table 2).

RESULTS

X-ray and neutron structural refinements

The X-ray diffraction data were first processed with the program E-STATISTICS, implemented in the WinGX package (Farrugia 1999). This program carries out a Wilson plot, calculates the

TABLE 2. Details of X-ray and neutron diffraction data collections and structural refinements of topaz

Crystal size (mm³)	0.160 × 0.110 × 0.020	2 × 3 × 13	2 × 3 × 13
Cell parameters	$a = 4.6601(2)$ Å	$a = 4.667(3)$ Å	$a = 4.641(9)$ Å
	$b = 8.8260(2)$ Å	$b = 8.834(4)$ Å	$b = 8.822(8)$ Å
	$c = 8.3778(2)$ Å	$c = 8.395(4)$ Å	$c = 8.382(9)$ Å
Z	4	4	4
T (K)	298	298	10
Radiation (Å)	MoKα	0.87238(1)	0.87238(1)
X-ray data collection			
2θ range (°)	2–70.12		
Scan type	ω		
Scan speed (°/s)	0.05		
Scan width (°)	1.20		
Neutron data collections			
Neutron flux density (n·s⁻¹·cm⁻²)		~2.5·10⁶	~2.5·10⁶
Scan type, steps, and width:			
10 < 2θ < 75°		31 steps, pure ω-scan	31 steps, pure ω-scan
75 < 2θ < 100°		31 steps, ω-2θ scan	31 steps, ω-2θ scan
Time per step (s)		5	5
u, v, w		5.4, −12.0, 16.3	5.4, −12.0, 16.3
Max. 2θ (°) and sinθ/λ	70.12, 0.8082	99.93, 0.8777	82.66, 0.7570
	0 ≤ h ≤ 7	−7 ≤ h ≤ 8	−7 ≤ h ≤ 7
	−5 ≤ k ≤ 14	−13 ≤ k ≤ 15	−13 ≤ k ≤ 13
	−13 ≤ l ≤ 13	−14 ≤ l ≤ 14	−10 ≤ l ≤ 12
No. measured reflections	1455	4446	4049
Space Group assignment:			
Prob. centrosymmetric structure	92.64%	82.94%	76.66%
$|E^2 - 1|$	0.988	0.932	0.915
CFOM-*Pbnm*	0.729	0.869	–
CFOM-*Pbn2₁*	9.178	4.226	–
Selected space group	*Pbmn*	*Pbmn*	*Pbmn*
No. unique reflections	725	988	632
No. unique refl. with $F_o > 4\sigma (F_o)$	718	892	600
No. refined parameters	47	57	57
Extinction correction factor	0.3294	0.3388	0.3817
R_{int}	0.0269	0.0229	0.0251
R_1 (F) with $F_o > 4\sigma (F_o)$	0.0195	0.0289	0.0391
R_1 (F) for all the unique refl.	0.0198	0.0361	0.0454
$wR_2 (F^2)$	0.0517	0.0627	0.0849
GooF	1.124	1.163	1.494
Weighting scheme: a, b	0.0065, 0.2023	0.0225, 1.1104	0.0209, 1.8720

Notes: $R_{int} = \Sigma|F_{obs}^2 - F_{obs}^2(mean)|/\Sigma(F_{obs}^2)$; $R_1 = \Sigma(|F_{obs}| - |F_{calc}|)/\Sigma|F_{obs}|$; $wR_2 = \{\Sigma[w(F_{obs}^2 - F_{calc}^2)^2]/\Sigma[w(F_{obs}^2)^2]\}^{0.5}$; · $w = 1/[\sigma^2(F_{obs}^2) + (a\cdot P)^2 + b\cdot P]$; $P = [Max(F_{obs}^2, 0) + 2\cdot F_{calc}^2]/3$. For neutron data collections: ω-scan width = $(u + v\cdot tanθ + w\cdot tan^2θ)^{0.5}$.

normalized structure factors (*E*-values) and the statistics of the distributions of these *E*-values. The structure of topaz was found to be centrosymmetric at 92.6%. In addition, even the Sheldrick's $|E^2 - 1|$ criterion (Sheldrick 1997) indicated that the structure is centrosymmetric ($|E^2 - 1| = 0.988$). Then, the diffraction data were processed with the program ASSIGN-SPACEGROUP (in WinGX, Farrugia 1999), which compares the equivalent reflections under all possible Laue symmetries, providing a valuable check on the supposed Laue symmetry. Two possible space groups (both belonging to the *mmm* Laue class) were selected by the program: *Pbmn* and *Pbn2₁*. However, the Combined Figure of Merit (CFOM) showed unambiguously that the space group *Pbmn* is highly likely (CFOM-*Pbmn* = 0.729, CFOM-*Pbn2₁* = 9.178; the lower the value of CFOM, the more likely the assignment is correct; a value below 10.0 indicates a satisfactory fit, whereas a value below 1.0 indicates that the suggested space group is highly likely). The crystal structure refinement was then performed in the space group *Pbmn* using the SHELX-97 software (Sheldrick 1997) with anisotropic thermal displacement

parameters and starting from the atomic coordinates of Alberico et al. (2003) without the H-position. Due to the low amount of the other elements present in the topaz sample (Table 1), only the (neutral) atomic scattering factors of Al, Si, and O have been used according to the *International Tables for Crystallography C* (Wilson and Prince 1999). At the end of the refinement, the final agreement index (R_1) was 0.0195 for 718 unique reflections with $F_o > 4\sigma(F_o)$ and 47 refined parameters (Table 2). No peak larger than $\pm 0.36\ e^-/Å^3$ was present in the final difference Fourier map. Further details concerning the structural refinement are reported in Table 2. Observed and calculated structure factors are reported in Table 3[1]. Atomic positions, bond distances and other relevant structural parameters are summarized in Tables 4 and 5.

The neutron diffraction data collected at room and low T were also processed with the aforementioned softwares of the WinGX suite. As for the X-ray diffraction data, the statistic criteria suggest that the structure is centrosymmetric with space group *Pbnm* (Table 2). The structural refinement with the diffraction data collected at room temperature was performed in space group *Pbnm* at first with isotropic displacement parameters using the SHELXL-97 package (Sheldrick 1997), starting with the atomic coordinates obtained from the X-ray structural refinement without the proton position. The neutron scattering lengths of Al, Si, and O from the *International Tables for Crystallography C* (Wilson and Prince 1999) were used. The secondary isotropic extinction effect was corrected according to Larson's formalism (1970), as implemented in SHELXL-97 package (Sheldrick 1997), using a fixed weighting scheme [$1/\sigma(F_o)^2$]. When convergence was achieved, one intense negative residual peak (–4.71 fm/Å³) at about $x = 0.496$, $y = 0.251$, $z = 0.164$ was found in the final difference-Fourier map of the nuclear density (Fig. 2). A further refinement was then performed assigning the H scattering length to this residual peak. The final least-square cycles were conducted with anisotropic displacement parameters and all the principal mean square atomic displacement parameters were positive definite. The occupancy factor of the proton site was fixed as a function of the oxygen at the F/O4-site (for the F/O4 site, %O = 100 – %F). A further test was performed allowing the occupancy of the proton site to vary without any restraint: the difference in occupancy, with respect to restrained one, was less than 2σ. At the end of the refinement, no peak larger than ± 0.84 fm/Å³ was found in the difference-Fourier map of the nuclear density and the final agreement index (R_1) was 0.0289 for 57 refined parameters and 892 unique reflections with $F_o > 4\sigma(F_o)$ (Table 2).

The neutron structural refinement based on the data collected at 10 K was conducted following the same protocol as the refinement at room T, using the refined site positions (including the

H-site) at room T as starting coordinates. The final agreement index (R_1) was 0.0391 for 600 unique reflections with $F_o > 4\sigma(F_o)$ and 57 refined parameters (Table 2). No peak larger than ± 1.02 fm/Å³ was found in the final nuclear difference-Fourier map. Site positions, occupancy factors and displacement parameters relative to the neutron structural refinements at room and low T are listed in Table 4. Bond distances and other relevant structural parameters are summarized in Tables 4 and 5. Observed and calculated structure factors are deposited (Table 3).[1]

Infrared spectra

Polarized mid-infrared spectra were collected over the region 5000–300 cm⁻¹ for examination of OH stretching and bending modes in the crystal structure of topaz. Four spectra were collected with the incident radiation polarized parallel to the crystallographic a (E//a) and c (E//c) axes using a thin section of the topaz crystal with the polished faces parallel to (010) and parallel to b (E//b) and c (E//c) using a thin section with the faces parallel to (100). Within the frequency range investigated, the E//b polarized IR spectra show only one sharp absorption band at 1161 cm⁻¹ (Fig. 3). In contrast, the E//a and E//c polarized
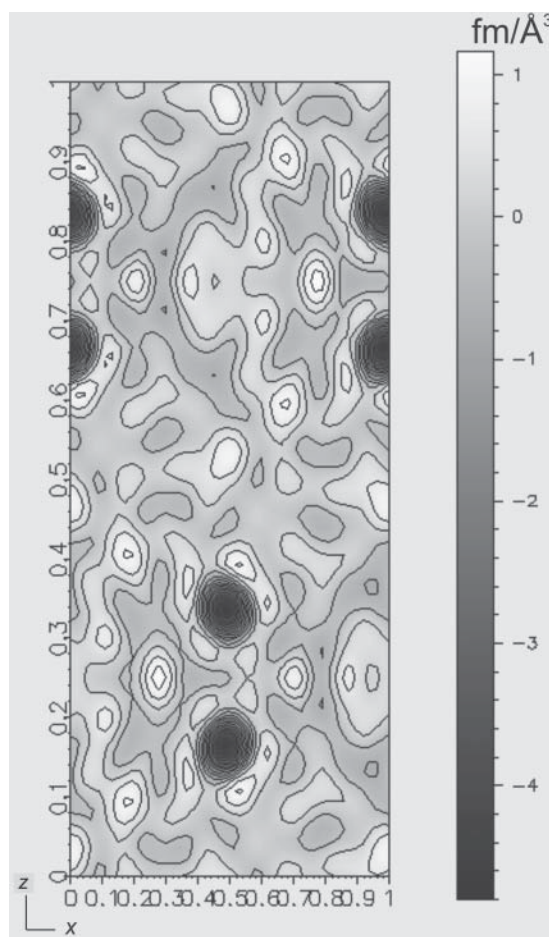
FIGURE 2. Difference (010) Fourier maps of the nuclear density of topaz at $y = 0.251$ after the first cycles of isotropic refinement with a proton-free structure. A strong negative residual peak of about –4.71 fm/ Å³ at $x = 0.496$ and $z = 0.164$ was found, ascribable to the H-position.

TABLE 4. Refined positional and displacement parameters (Å^2) of topaz

	x	y	z	occ	U_{11}	U_{22}	U_{33}	U_{23}	U_{13}	U_{12}	U_{eq}
Al	0.9053(6)	0.13131(3)	0.0816(3)	1	0.0034(1)	0.0040(1)	0.00436(8)	0.00008(8)	−0.00010(8)	0.00008(8)	0.0039(1)
(8d)	0.9051(1)	0.13123(8)	0.0817(1)	1	0.0037(2)	0.0026(2)	0.0048(3)	0.0002(2)	−0.00001(1)	0.0002(1)	0.0037(1)
	0.9056(3)	0.1313(1)	0.0817(2)	1	0.0028(5)	0.0013(5)	0.0047(6)	0.0006(4)	−0.0005(4)	0.0003(4)	0.0029(3)
Si	0.39976(7)	0.94088(4)	1/4	1	0.0027(2)	0.0036(2)	0.0038(1)	0	0	0.0001(1)	0.0033(1)
(4c)	0.3996(2)	0.94088(8)	1/4	1	0.0026(2)	0.0020(2)	0.0045(3)	0	0	0.0003(2)	0.0030(1)
	0.3996(2)	0.9409(2)	1/4	1	0.0018(6)	0.0010(5)	0.0052(7)	0	0	0.0003(5)	0.0027(3)
O1	0.7064(2)	0.0311(1)	1/4	1	0.0041(3)	0.0054(3)	0.0054(3)	0	0	0.0017(3)	0.005(2)
(4c)	0.7059(1)	0.03129(7)	1/4	1	0.0038(2)	0.0041(2)	0.0054(2)	0	0	−0.0011(1)	0.0045(1)
	0.7069(2)	0.0312(1)	1/4	1	0.0039(5)	0.0026(5)	0.0050(5)	0	0	−0.0004(3)	0.0038(3)
O2	0.4516(2)	0.7564(1)	1/4	1	0.0059(3)	0.0037(3)	0.0050(3)	0	0	0.0009(2)	0.0049(2)
(4c)	0.4529(1)	0.75627(7)	1/4	1	0.0055(2)	0.0026(2)	0.0057(2)	0	0	0.0008(1)	0.0046(1)
	0.4528(3)	0.7562(1)	1/4	1	0.0042(5)	0.0014(4)	0.0062(5)	0	0	0.0012(3)	0.0039(3)
O3	0.2114(1)	0.98979(7)	0.09284(7)	1	0.0046(2)	0.0047(2)	0.0047(2)	−0.0003(2)	−0.0011(2)	0.0007(2)	0.0047(1)
(8d)	0.2114(1)	0.98961(5)	0.09270(5)	1	0.0043(1)	0.0037(1)	0.0054(2)	−0.0002(1)	−0.0011(1)	0.0008(1)	0.0045(1)
	0.2117(2)	0.9899(1)	0.0926(1)	1	0.0031(3)	0.0020(3)	0.0061(4)	0.0001(2)	−0.0006(2)	0.0006(2)	0.0037(2)
F/O4	0.5928(1)	0.25263(7)	0.05988(7)	1	0.0075(2)	0.0084(2)	0.0089(2)	0.0013(2)	0.0005(2)	−0.0023(2)	0.0083(1)
(8d)	0.5976(1)	0.25265(5)	0.05971(6)	0.78(1)	0.0060(2)	0.0056(2)	0.0084(2)	0.0010(1)	−0.0008(1)	0.0022(1)	0.0067(1)
	0.5973(2)	0.2525(1)	0.0599(1)	0.79(1)	0.0040(4)	0.0028(4)	0.0071(4)	−0.0001(2)	−0.0003(2)	0.0008(2)	0.0047(2)
H	–	–	–	–	–	–	–	–	–	–	–
(8d)	0.495(2)	0.252(1)	0.1629(7)	0.22(1)	0.041(4)	0.049(4)	0.019(2)	0.014(2)	0.015(2)	0.026(3)	0.037(2)
	0.492(2)	0.251(1)	0.1637(1)	0.21(1)	0.027(5)	0.027(5)	0.022(5)	0.008(4)	0.015(4)	0.010(3)	0.025(3)

Notes: For each site, values from top to bottom correspond to the X-ray structural refinement at 298 K, neutron refinement at 298 and 10 K, respectively. The occupancy factor (o.c.) of the F/O4 site (occupied by fluorine and oxygen) corresponds to the fluorine content ($O_{o.c.} = 1 − F_{o.c.} = H_{o.c.}$). For the X-ray structural refinement, the F/O4 site was considered fully occupied by F. The anisotropic displacement factor exponent takes the form: $−2\pi^2[(ha^*)^2U_{11} + ... + 2hka^*b^*U_{12}]$. U_{eq} is defined as one-third of the trace of the orthogonalized U_{ij} tensor.

IR spectra show two absorption bands at 3640 and 1161 cm^{-1}, the first prominent for E//c and the second prominent for E//a (Fig. 3). Frequencies of these two absorption bands are in good agreement, and absorption band anisotropies are in excellent agreement with the IR data presented by Shinoda and Aikawa (1997). According to Shinoda and Aikawa (1997), the IR-active bands at 3640 and at 1161 cm^{-1} can be ascribed to OH-stretching and OH-bending modes, respectively. The strong pleochroism of the OH-stretching mode (at 3640 cm^{-1}), which has no component of vibration parallel to the b axis (Fig. 3), suggests that the O-H direction is perpendicular to [010] [i.e., the hydroxyl group lies on the (010)-plane]. In contrast, the nature of the OH-bending mode (at 1161 cm^{-1}), which has components along all three crystallographic axes (more prominent along a and b than along c), provides a clue for the motion of the OH-group and in particular on the anisotropic displacement of the proton, which will be discussed and compared with the neutron structural refinement finding.

The IR-investigation of this natural topaz shows that neither molecular H_2O nor CO_2 are present in the structure, and that all hydrogen is present as OH$^-$ groups.

DISCUSSION AND CONCLUSIONS

The single-crystal X-ray and neutron diffraction data collected in this study allow us to infer that the crystal structure of natural topaz with OH/(OH + F) < 0.5 can be described with the *Pbnm* space group. Reflections violating the *Pbnm* symmetry, found in previous investigations and in this study, are likely due to Renninger effect (double diffraction phenomenon). Several recent studies have demonstrated that the probability of occurrence of geometric conditions for double diffraction is high. Concerning minerals, two interesting examples can be found regarding the real symmetry of pyrope (Rossmanith and Armbruster 1995) and stibnite (Sørensen and Lundegaard 2004).

The reason for the optical anomalies of natural topaz observed by Akizuki et al. (1979) are still unclear, but in recent years a high number of studies have shown that the optical properties

TABLE 5. Relevant structural parameters of topaz as refined on the basis of X-ray and neutron diffraction data

	X-ray data T = 298 K	Neutron data T = 298 K	Neutron data T = 10 K
Al-F/O4 (Å)	1.7969(6)	1.801(1)	1.795(3)
Al-F/O4 (Å)	1.8059(6)	1.808(1)	1.803(2)
Al-O1 (Å)	1.9056(7)	1.908(1)	1.903(2)
Al-O2 (Å)	1.9116(7)	1.912(1)	1.907(2)
Al-O3 (Å)	1.8904(7)	1.892(1)	1.890(2)
Al-O3 (Å)	1.8986(7)	1.902(1)	1.892(3)
F/O4-H (Å)	–	0.989(5)	0.997(9)
<Al-F/O> (Å)	1.8682	1.870	1.865
O1-Al-O2 (°)	83.75(3)	83.63(5)	83.49(11)
O1-Al-O3 (°)	91.35(4)	91.48(5)	91.27(11)
O1-Al-O3' (°)	99.79(3)	99.90(5)	99.84(11)
O1-Al-F/O4 (°)	87.93(4)	87.89(5)	88.01(12)
O2-Al-O3 (°)	94.65(4)	94.80(5)	94.97(11)
O2-Al-F/O4 (°)	90.50(4)	90.45(5)	90.33(11)
O2-Al-F/O4' (°)	89.04(3)	89.16(5)	89.33(11)
O3-Al-O3 (°)	83.26(3)	83.25(4)	83.14(10)
O3-Al-F/O4 (°)	91.69(3)	91.58(5)	91.65(10)
O3-Al-F/O4' (°)	87.51(3)	87.41(5)	87.47(11)
O3-Al-F/O4'' (°)	91.83(3)	91.82(5)	92.08(12)
F/O4-Al-F/O4 (°)	89.54(2)	89.47(5)	89.30(12)
Si-O1 (Å)	1.6360(10)	1.638(1)	1.634(3)
Si-O2 (Å)	1.6461(9)	1.650(1)	1.648(2)
Si-O3 (×2) (Å)	1.6402(7)	1.643(1)	1.640(2)
<Si-O> (Å)	1.6406	1.643	1.640
O1-Si-O2 (°)	110.71(5)	110.51(6)	110.58(13)
O1-Si-O3 (°)	109.82(3)	109.80(4)	109.62(10)
O2-Si-O3 (°)	109.81(3)	109.85(4)	109.90(7)
O3-Si-O3 (°)	106.79(5)	106.95(7)	107.15(15)
F/O4···F/O4 (Å)	3.186(2)	3.195(3)	3.187(9)
H···O1 (Å)	–	2.307(6)	2.297(6)
H···O2 (Å)	–	2.216(5)	2.190(9)
H···O3 (Å)	–	2.380(5)	2.386(6)
H···F/O4 (Å)	–	2.377(5)	2.368(6)
H···H (Å)	–	1.463(5)	1.448(6)
F/O4-H···O1	–	94.2(4)	94.2(6)
F/O4-H···O2	–	138.2(5)	138.5(7)
F/O4-H···O3	–	88.7(4)	88.0(6)
F/O4-H···F/O4	–	139.5(5)	138.9(7)
Al-F/O4-H (°)	–	107.1(1)	107.1(2)
Al-F/O4-H' (°)	–	109.6(1)	109.9(2)

of minerals might lead to a wrong determination of symmetry, because they are strongly influenced by tectonic stress, anomalous solid solutions series, incorporation of trace elements, and/or rough preparation methods of the thin sections (Libowitzky 1991,
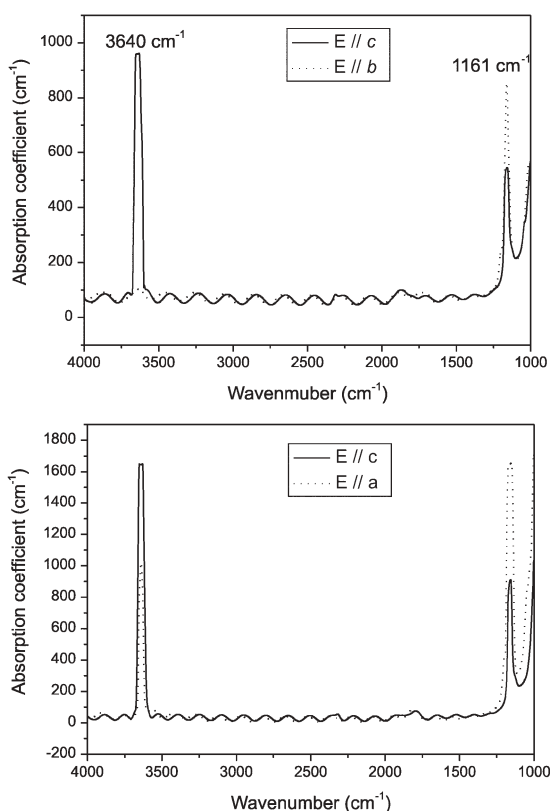
FIGURE 3. Polarized single-crystal IR spectra of natural topaz in the region between 4000–1000 cm^{-1}, (above) with the incident radiation polarized parallel to the b (E//b) and c (E//c) axes [using a thin section with the polished faces parallel to (100)] and (below) parallel to a (E//a) and c (E//c) [thin section with the faces parallel to (010)].

1994a, 1994b, 1994c, 1994d, 2001; Kahr and McBride 1992 and references therein; Tanaka et al. 2002; Baur and Fisher 2003). An interesting critical review concerning the real symmetry of some minerals, erroneously assigned on the basis of optical investigations, is given in Baur and Fisher (2003).

The site positions refined in this study by means of single-crystal X-ray and neutron diffraction are in good agreement with those reported by Zemann et al. (1979) for a natural Al$_2$SiO$_4$(F$_{1.44}$OH$_{0.56}$) topaz, with differences of <2σ. The refined tetrahedral and octahedral bond distances and angles show quite regular polyhedra. Ribbe and Gibbs (1971) explained the small distortions of the polyhedra in the topaz structure with respect to ideal polyhedra in closest-packed structures in terms of simple electrostatic interactions. The F-amount of our sample refined on the basis of the neutron diffraction data (1.54–1.60 apfu, 14.6–15.2 wt% Table 4) appears to be slightly lower than that measured by means of WDS-EMPA [17.66(12) wt%, Table 1] and that determined by the correlation equation between F wt% and unit-cell constants [16.97(6) wt%, following Alberico et al. 2003]. The nuclear density Fourier map shows that the proton is located at the Wyckoff 8d position and the refined coordinates are: $x = 0.495(2)$, $y = 0.252(1)$, $z = 0.1629(7)$ (Table 4). The O-H bond lies on the (010)-plane and forms an angle of about 28.9° with the c-axis (Fig. 4). The neutron structural refinement

shows that at room conditions the displacement ellipsoid of the proton is highly anisotropic (with the principal RMS-displacement parameters as 2.67:1.32:1). At 10 K this anisotropy slightly decreases (principal RMS-parameters as 2.24:1.42:1) and the U_{eq} parameter is reduced by about 30%. The refined bond distances and angles between the proton site and the surrounding anions imply that at least four potential weak H⋯O/F interactions occur (i.e., H⋯O1, H⋯O2, H⋯O3, and H⋯F/O4, Fig. 5, Table 5), where one (i.e., H⋯O2) is slightly stronger than the others. The hydrogen-bonding observed at room T is maintained at low T (Table 5). The topological configuration of the proton described in this study for natural topaz with OH/(OH + F) ≤ 0.5 differs from that of the (synthetic) topazes with OH/(OH + F) > 0.5 (hereafter "topaz-OH"), where two non-equivalent and partially occupied H-sites are present and where the proton ordering might imply reduction of the symmetry to the $Pbn2_1$ space group (with a loss of the mirror plane), dictated by the proton-proton avoidance rule (Northrup et al. 1994; Chen et al. 2005). In fact, for the topaz-OH each of the two non-equivalent proton sites (i.e., H1 and H2) is characterized by an irregular trifurcated hydrogen-bond geometry [H1⋯O2, H1⋯O3, and H1⋯O4 with refined hydrogen-bond distances in the range 2.038(5)–2.281(6) Å; H2⋯O1, H2⋯O2, and H2⋯O4 with distances in the range 2.280(5)–2.524(5) Å, Chen et al. 2005], with the weaker bonds associated to H2. In this light, we can infer that the topological configuration of the proton site in natural topazes with OH/(OH + F) ≤ 0.5 appears to be an "average configuration" with respect to the H1 and H2 sites in topaz-OH. In fact, for the natural topaz of this study the refined hydrogen-bond distances lie in the range 2.216(5)–2.380(5) Å (Table 5) with four anions bonded. In other words, the "framework" of the crystal structure of topaz is maintained along the join Al$_2$SiO$_4$F$_2$-Al$_2$SiO$_4$(OH)$_2$ and only the topological configuration of the proton site/sites changes. Such structural re-arrangement is possible due to the presence of the aforementioned cavity, which allows the presence of two independent proton sites in topaz-OH without any drastic change in the framework. However, the different topological configuration of the proton site(s) in topaz structure implies different phase stability conditions. In fact, studies of natural and synthetic topaz appear to confirm that the stability of topaz-OH is restricted to very high-pressure/high-temperature conditions (Barton 1982; Wunder et al. 1993, 1999; Northrup et al. 1994; Schmidt et al. 1998; Zhang et al. 2002; Chen et al. 2005). In contrast, natural F-rich topaz [with OH/(OH + F) ≤ 0.5] can be found as accessory mineral in F-rich granitic rocks and associated with pneumato-lithic/hydrothermal events.

The topological configuration of the OH-group described by the neutron structural refinements is confirmed by the IR investigation: the OH-stretching mode (at 3640 cm^{-1}) has no component of vibration parallel to the b axis (Fig. 3), therefore the O-H direction is perpendicular to [010] (Fig. 4). The OH-bending mode (at 1161 cm^{-1}) shows components along the three crystallographic axes, which appear to be more prominent along the a- and b-axes than along the c-axis (Fig. 3). The magnitude and orientation of the thermal displacement ellipsoid of the proton, based on the neutron structure refinements, supports the vibrational evidence because the major components of the three principal thermal ellipsoid coefficients along the crystallographic
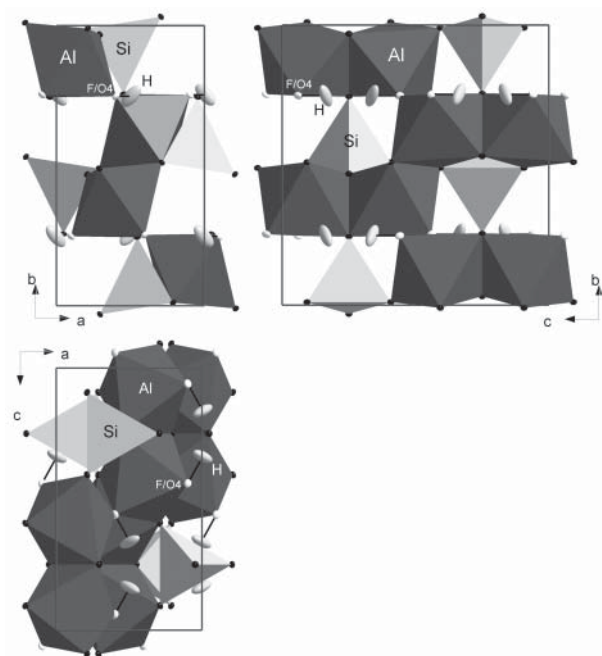
FIGURE 4. Crystal structure of topaz based on the neutron structural refinement at 298 K, viewed down [100], [010], and [001]. Thermal ellipsoid probability: 50%.

FIGURE 5. Topological configuration of the OH-group and hydrogen-bonding arrangement based on the neutron structural refinement. Bond distances and angles are listed in Table 5.

axes are parallel to a and b (Fig. 4) (the projection of the principal RMS-displacement parameters along the a-, b-, and c-axis at 298 K are respectively as 1.5:1.6:1). The wavenumber position of the OH stretching frequency in topaz spectra (3640 cm^{-1}) and its relatively narrow bandwidth are consistent with weak (or absent) hydrogen bonding in the topaz structure. This is in agreement with the structural data concerning the topological configuration of the proton site (Table 5) discussed above.

Previous studies have reported the presence of Fe and Cr substituting Al in the octahedral site and As for Si in the tetrahedral site (Ribbe and Rosenberg 1971; Ribbe 1982; Northrup and Reeder 1994). Also the presence of Co, Ni, V, Mn, Ga, and Cu impurities have been reported for natural topaz (Ribbe 1982 and references therein; Northrup and Reeder 1994). In this study, we found also the presence of Na (~240 wt ppm) and Ca (~634 ppm) in an amount larger than that of Fe (~24 ppm), Cr (~67 ppm), and V (~7 ppm) (Table 1). Na and Ca might substitute Al in distorted polyhedra with CN > 6. Such local distortions can be accommodated because of the presence of cavities adjacent to the Al(O,F,OH)$_6$-octahedra (where the protons lie). More likely, these alkaline and earth-alkaline cations would be located in the cavities substituting the protons, with a zeolite-like extra-framework configuration. In addition, a low amount of Ti (~56 ppm) has been found (Table 1), which might replace either Al or Si in the octahedral/tetrahedral sites. B (~13 ppm, Table 1) likely occupies in the tetrahedral site replacing Si. Substitution of various cations into the octahedral site in topaz would be expected to influence the OH stretching frequencies due to the next-nearest-neighbor (NNN) effects, and would either result in broadening of the OH stretching band, or in the appearance of additional OH stretching modes in the IR spectra. However, the
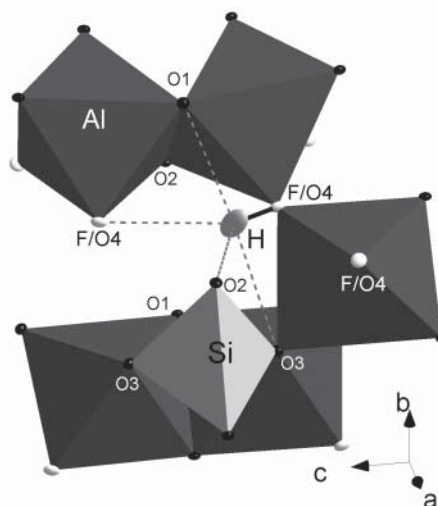
concentration of additional elements in our sample is too small, and the amount of OH present too high, for any such effects to be noticeable.

REFERENCES CITED

Akizuki, M., Hampar, M.S., and Zussman, J. (1979) An explanation of anomalous optical properties of topaz. Mineralogical Magazine, 43, 237–241.

Alberico, A., Ferrando, S., Ivaldi, G., and Ferraris, G. (2003) X-ray single-crystal structure refinement of an OH-rich topaz from Sulu UHP terrane (Eastern China)—Structural foundation of the correlation between cell parameters and fluorine content. European Journal of Mineralogy, 15, 875–881.

Alston, N.A. and West, J. (1928) The structure of topaz. Proceedings of the Royal Society, A121, 358–367.

Angel, R.J. (2002) ABSORB V5.2. Computer program. Crystallography Laboratory, Department Geological Sciences, Virginia Tech, Blacksburg.

——— (2003a) Automated profile analysis for single-crystal diffraction data. Journal of Applied Crystallography, 36, 295–300.

——— (2003b) WIN-INTEGRSTPV3.4. Computer program. Crystallography Laboratory, Department Geological Sciences, Virginia Tech, Blacksburg.

Angel, R.J., Downs, R.T., and Finger, L.W. (2000) High-Temperature-High-Pressure Diffractometry. In R.M. Hazen and R.T. Downs, Eds., High-Temperature and High-Pressure Crystal Chemistry, 41, p. 559–596. Reviews in Mineralogy and Geochemistry, Mineralogical Society of America, Chantilly, Virginia.

Barton, M.D. (1982) The thermodynamic properties of topaz solid solution and some petrological applications. American Mineralogist, 67, 956–974.

Barton, M.D., Haselton, H.T., Jr, Hemingway, B.S., Kleppa, O.J., and Robie, R.A. (1982) The thermodynamic properties of fluor-topaz. American Mineralogist, 67, 350–355.

Baur, W.H. and Fisher, R.X. (2003) On the significance of small deviations from higher symmetry. Mineralogical Magazine, 67, 793–797.

Belokoneva, E.L., Smirnitskaya, Y.Y., and Tsirel'son, V.G. (1993) Electron density distribution in topaz Al$_2$[SiO$_4$](F,OH)$_2$ as determination from high-precision X-ray diffraction data. Russian Journal of Inorganic Chemistry, 38-8, 1252–1256.

Bradbury, S.E. and Williams, Q. (2003) Contrasting bonding behavior of two hydroxyl-bearing metamorphic minerals under pressure: clinozoisite and topaz. American Mineralogist, 88, 1460–1470.

Burnham, C.W. (1966) Computation of absorption corrections and the significance of end effects. American Mineralogist, 51, 159–167.

Chen, J., Lager, G.A., Kunz, M., Hansen, T., and Ulmer, P. (2005) A Rietveld

refinement using neutron powder diffraction data of a fully deuterated topaz, $Al_2SiO_4(OD)_2$. Acta Crystallographica, E61, i253–i255.

Churakov, S.V. and Wunder, B. (2004) Ab-initio calculations of the proton location in topaz-OH, $Al_2SiO_4(OH)_2$. Physics and Chemistry of Minerals, 31, 131–141.

Domanik, K.J. and Holloway, J.R. (1996) The stability and composition of phengitic muscovite and associated phases from 5.5 to 11 GPa: Implications for deeply subducted sediments. Geochimica and Cosmochimica Acta, 60, 4133–4150.

Farrugia, L.J. (1999) WinGX suite for small-molecule single-crystal crystallography. Journal of Applied Crystallography, 32, 837–838.

Gatta, G.D., Nestola, F., and Boffa Ballaran, T. (2006a) Elastic behaviour and structural evolution of topaz at high pressure. Physics and Chemistry of Minerals, 33, 235–242.

Gatta, G.D., Nestola, F., Bromiley, G.D., and Mattauch, S. (2006b) The real topological configuration of the extra-framework content in alkali-poor beryl: a multi-methodological study. American Mineralogist, 91, 29–34.

Holland, T.J.B., Redfern, S.A.T., and Pawley, A.R. (1996) Volume behaviour of hydrous minerals at high pressures and temperature; II, Compressibility of lawsonite, zoisite, clinozoisite, and epidote. American Mineralogist, 81, 341–348.

Isetti, G. and Penco, A.M. (1967) La determinazione della posizione dell'idrogeno nell'ossidril-topazio mediante la spettrofotometria infrarossa in luce polarizzata. Periodico di Mineralogia (Roma), 36, 995–1010.

Kahr, B. and McBride, J.M. (1992) Optically anomalous crystals. Angewandte Chemie International Edition, 31, 1–26.

King, H.E. and Finger, L.W. (1979) Diffracted beam crystal centering and its application to high-pressure crystallography. Journal of Applied Crystallography, 12, 374–378.

Komatsu, K., Kuribayashi, T., and Kudoh, Y. (2003) Effect of temperature and pressure on the crystal structure of topaz, $Al_2SiO_4(OH,F)_2$. Journal of Mineralogical and Petrological Sciences, 98, 167–180.

Komatsu, K., Kagi, H., Okada, T., Kuribayashi, T., Parise, J.B., and Kudoh, Y. (2005) Pressure dependence of the OH-stretching mode in F-rich natural topaz and topaz-OH. American Mineralogist, 90, 266–270.

Ladell, J. (1965) Redetermination of the crystal structure of topaz: a preliminary account. Norelco Reporter, 12, 34–39.

Larson, A.C. (1970) Crystallographic Computing (F.R. Ahmed, S.R. Hall, and C.P. Huber, Eds.), p. 291–294. Munksgaard, Copenhagen, Denmark.

Libowitzky, E. (1991) Donathite: An intergrowth of magnetite and chromite, causing form birefringence. Neues Jahrbuch für Mineralogie Monatshefte, 1991, 449–456.

——— (1994a) Anisotropic pyrite: A polishing effect. Physics and Chemistry of Minerals, 21, 97–103.

——— (1994b) Optical anisotropy of cuprite caused by polishing. Canadian Mineralogist, 32, 353–358.

——— (1994c) Optical anisotropy in the spinel group: A polishing effect. European Journal of Mineralogy, 6, 187–194.

——— (1994d) Optical anisotropy of zoned magnetites due to form birefringence. Mineralogy and Petrology, 52, 107–111.

——— (2001) The pseudo-biabsorption of trigonal rock-forming carbonates. Neues Jahrbuch für Mineralogie Monatshefte, 2001, 67–79.

Longerich, H.P., Jackson, S.E., and Günther, D. (1996) Laser ablation-inductively coupled plasma mass spectrometric transient signal data acquisition and analyte concentration calculation. Journal of Analytical Atomic Spectroscopy, 11, 899–904.

Northrup, P.A. and Reeder, R.J. (1994) Evidence for the importance of growth-surface structure to trace element incorporation in topaz. American Mineralogist, 79, 1167–1175.

Northrup, P.A., Leinenweber, K., and Parise, J.P. (1994) The location of H in the high-pressure synthetic $Al_2SiO_4(OH)_2$ topaz analogue. American Mineralogist, 79, 401–404.

Parise, J.B., Cuff, C., and Moore, F.H. (1980) A neutron diffraction study of topaz:

evidence for lower symmetry. Mineralogical Magazine, 43, 943–944.

Pauling, L. (1928) The crystal structure of topaz. Proceedings of the National Academy of Sciences of the United States of America, 14, 603–606.

Pichavant, M. and Manning, D. (1984) Petrogenesis of tourmaline granites and topaz granites: the contribution of experimental data. Physics of the Earth and Planetary Interiors, 35, 31–50.

Ralph, R.L. and Finger, L.W. (1982) A computer program for refinement of crystal orientation matrix and lattice constants from diffractometer data with lattice symmetry constraints. Journal of Applied Crystallography, 15, 537–539.

Ribbe, P.H. (1982) Topaz. In P.H. Ribbe, Ed., Orthosilicates (2nd edition), 5, p. 215–230. Reviews in Mineralogy, Mineralogical Society of America, Chantilly, Virginia.

Ribbe, P.H. and Gibbs, G.V. (1971) The crystal structure of topaz and its relation to physical properties. American Mineralogist, 56, 24–30.

Ribbe, P.H. and Rosenberg, P.E. (1971) Optical and X-ray determinative methods for fluorine in topaz. American Mineralogist, 57, 168–187.

Rinne, F. (1926) Bemerkingen über optische Anomalien, insbesondere des brasilianer Topas. Zeitschrift für Kristallographie, 63, 236–246.

Rossmanith, E. and Armbruster, T. (1995) The intensity of forbidden reflections of pyrope: Umweganregung or symmetry reduction? Zeitschrift für Kristallographie, 210, 645–649.

Schmidt, M.W., Finger, L.W., Angel, R.J., and Dinnebier, R.E. (1998) Synthesis, crystal structure and phase relations of $AlSiO_3OH$, a high-pressure hydrous phase. American Mineralogist, 83, 881–888.

Sheldrick, G.M. (1997) SHELX-97. Programs for crystal structure determination and refinement. Institute of Inorganic Chemistry, University of Göttingen, Germany.

Shinoda, K. and Aikawa, N. (1997) IR active orientation of OH bending mode in topaz. Physics and Chemistry of Minerals, 24, 551–554.

Sørensen, H.O. and Lundegaard, L.F. (2004) On the space-group dispute of stibnite. Journal of Applied Crystallography, 37, 156–158.

Tanaka, T., Kimura, R., Akizuki, M., and Kudoh, Y. (2002) Origin of low-symmetry growth vectors in edingtonite and yugawaralite, and crystal structure of the k{011} and v{120} sectors of yugawaralite. Mineralogical Magazine, 66, 409–420.

Taylor, R.P. (1992) Petrological and geochemical characteristics of the Pleasant Ridge zinnwaldite-topaz granite, southern New Brunswick, and comparisons with other topaz-bearing felsic rocks. Canadian Mineralogist, 30, 895–921.

Taylor, R.P. and Fallick, A.E. (1997) The evolution of fluorine-rich felsic magmas: source dichotomy, magmatic convergence, and the origins of topaz granite. Terra Nova, 9, 105–108.

Wilson, A.J.C. and Prince, E., Eds. (1999) International Tables for X-ray Crystallography, Volume C: Mathematical, physical and chemical tables (2nd Edition). Kluwer Academic, Dordrecht.

Wunder, B., Rubie, D.C., Ross, C.R., Medenbach, O., Seifert, F., and Schreyer W. (1993) Synthesis, stability, and properties of $Al_2SiO_4(OH)_2$: a fully hydrated analogue of topaz. American Mineralogist, 78, 285–297.

Wunder, B., Andrut, M., and Wirth, R. (1999) High-pressure synthesis and properties of OH-rich topaz. European Journal of Mineralogy, 11, 803–813.

Zemann, J., Zobetz, E., Heger, G., and Völlenke, H. (1979) Strukturbestimmungeines OH-reichen Topases. Anzeiger der Österreichische Akademie der Wissenschaften (Mathematisch-Naturwissenschaftliche Klasse), 116(6), 145–147.

Zhang, R.Y., Liou, J.G., and Shu, J.F. (2002) Hydroxyl-rich topaz in high-pressure and ultrahigh-pressure kyanite quartzites, with retrograde woodhouseite, from the Sulu terrane, eastern China. American Mineralogist, 87, 445–453.